Astroparticle Physics 34 (2010) 187–197

Contents lists available at ScienceDirect

Astroparticle Physics

journal homepage: www.elsevier.com/locate/astropart

Water transparency measurements in the deep Ionian Sea *

E.G. Anassontzis [a,*], A.E. Ball [b,c], A. Belias [c], A. Fotiou [c], G. Grammatikakis [d], H. Kontogiannis [e], P. Koske [f], S. Koutsoukos [c], V. Lykoussis [e], E. Markopoulos [c], A. Psallidas [c], L.K. Resvanis [a,c], I. Siotis [g], S. Stavrakakis [e], G. Stavropoulos [c], V.A. Zhukov [h,i]

[a] Physics Department, University of Athens, Athens, Greece
[b] Formerly of CERN (European Organization for Nuclear Research), Geneva, Switzerland
[c] NESTOR Institute for Deep Sea Research, Technology and Neutrino Astroparticle Physics, National Observatory of Athens, Pylos, Greece
[d] Physics Department, University of Crete, Greece
[e] Institute of Oceanography, Hellenic Center for Marine Research, Anavyssos, Greece
[f] Institute of Experimental and Applied Physics, University of Kiel, Kiel, Germany
[g] Institute of Nuclear Physics, National Center for Scientific Research 'Demokritos', Athens, Greece
[h] Institute For Nuclear Research, Russian Academy of Sciences, Moscow, Russia
[i] Moscow State Open University, Moscow, Russia

ARTICLE INFO

Article history:
Received 1 April 2010
Received in revised form 26 June 2010
Accepted 27 June 2010
Available online 3 July 2010

Keywords:
Neutrino
Underwater telescope
KM3NeT
NESTOR
Water transparency

ABSTRACT

A long optical base line spectrophotometer designed to measure light transmission in deep sea waters is described. The variable optical path length allows measurements without the need for absolute or external calibration. The spectrophotometer uses eight groups of uncollimated light sources emitting in the range 370–530 nm and was deployed at various depths at two locations in the Ionian Sea that are candidate sites for a future underwater neutrino telescope. Light transmission spectra at the two locations are presented and compared.

* I have included this paper in my publications since I directed and carried out most of the analysis and the writing of this work. I withdrew my name in protest over the capricious behaviour of Prof. Leo Resvanis in excluding from the author list persons that significantly contributed in this work, while at the same time including people that had hardly contributed to this effort.

Petros A. Rapidis, Institute of Nuclear Physics, NCSR 'Demokritos'

1. Introduction

The study of high energy neutrinos of astrophysical origin requires the use of very large target masses, in order to observe a reasonable number of neutrino interactions given the small interaction cross-section for neutrino-nucleon scattering. The observation, mainly via the production of muons, relies on the detection of the Cherenkov radiation produced and thus requires an optically transparent target material. Such large amounts of target material can be most easily obtained by using naturally abundant and transparent media, such as water or ice. Currently the world's largest neutrino telescope, IceCube [1], is nearing completion at the South Pole and will encompass one cubic kilometre of glacial ice in its final configuration. In contrast, the proposed KM3NeT detector (Kilometer cube Neutrino Telescope) [2], a neutrino telescope planned to be a few times larger than IceCube, will be deployed in the Mediterranean Sea and thus will use sea water as its detection medium.

In charged current interactions of muon–neutrinos with sea water or underlying rock, the produced high-energy muons travel faster than the speed of light in water and thus emit Cherenkov light that provides the primary observation mode of such a detector. Muons lose very little energy as they travel through matter, and thus have a very long range (e.g. $\approx$7.8 km for $E_\mu = 10$ TeV). They can therefore be produced far from the detector and still be observed. As a result the effective interaction target volume is equal to the cross sectional area of the detector multiplied by the muon range.

The detector itself will consist of a three dimensional lattice of photomultipliers that detect the Cherenkov light and record the time of its arrival and its amplitude. This information is used to reconstruct the direction of the muon, to obtain a rough estimate of its energy and thus to extract a measure of the parent neutrino direction and energy. The photomultipliers are contained in glass spheres capable of withstanding high pressure. These so-called 'optical modules' (OM) are deployed at great depth where there is no ambient light.

* Corresponding author. Address: N&K University of Athens, Faculty of Physics, Nuclear and Particle Physics Department, Panepistimioupolis, Ilissia GR-15771, Athens, Greece. Tel./fax: +30 210 7276948.
E-mail address: eanason@phys.uoa.gr (E.G. Anassontzis).

0927-6505/$ - see front matter © 2010 Elsevier B.V. All rights reserved.
doi:10.1016/j.astropartphys.2010.06.008

Upwards moving and near horizontal muons arising from neutrino interactions in the surrounding earth or water are one of the primary signals in such a neutrino telescope. For neutrinos arriving from below the horizon, the earth serves as a shield against cosmic ray-induced muons. For very high energy neutrinos (>50 TeV), the earth also attenuates the neutrino flux, and for energies above 500 TeV it is essentially opaque. For a neutrino telescope deployed at a large depth (>4 kmwe) the surrounding water attenuates the downwards moving (background) cosmic ray-induced muons, and provides an enhanced solid angle for very high energy neutrinos thus allowing the detection of neutrinos coming from small zenith angles (i.e. coming from directly above) and all the way down to the horizon. This shift from neutrino sensitivity for upwards moving neutrinos at lower energies to downwards moving neutrinos at higher energy is accompanied by a flux reduction which is somewhat compensated by the increasing neutrino cross-section. This however only applies to detectors sufficiently deep to take advantage of the cosmic ray shielding provided by a large overburden.

The spacing between the optical modules is determined by the transparency of the sea water. Greater water transparency allows for a sparser detector, leading to a larger detector mass and cross-sectional area for the same number of deployed optical modules. As a result, the selection of a deployment site with the clearest waters is of paramount importance in the construction of a large underwater neutrino telescope if one wants to maximize the detector's sensitivity for given resources. Since the spacing between optical modules will scale with some characteristic water transparency length, *a fortiori*, the effective volume of a detector, for a fixed number of optical modules, will depend on the water transparency. The exact scaling of such detector properties will have to be determined by detailed Monte-Carlo simulation studies. Optical scattering of the Cherenkov radiation affects the angular resolution of such telescopes. In sum, the energy and angular resolution of the detector depends on the optical properties of the water and a precise knowledge of them is required for a proper interpretation of the experimental data.

In the Ionian Sea, two candidate areas are under investigation for deploying the KM3NeT: the Pylos area, with a series of plateaus at depths of 3000, 3750, 4550, and 5200 m, located at distances of 13–48 km from shore, SW of the city of Pylos, Greece and the Capo Passero area, with depth of 3600 m, located at a distance of 77–102 km from shore, SE of Capo Passero, the most south-eastern cape of Sicily, Italy. The Pylos area is where the NESTOR collaboration [3] has operated until now and where a section of the NESTOR neutrino telescope tower has been deployed. The Capo Passero area is where the NEMO collaboration [4] has been active. We have taken measurements of the water clarity at four different sites, two within the Pylos area (N4.5D and N5.2D) and two within the Capo Passero area (CP1 and CP2) and on three different campaigns; the dates, coordinates and depths of these sites/measurements are shown in Table 1. The deployment campaigns were conducted by the Research Vessel 'Aegaeo' of the Hellenic Centre for Marine Research.

2. Experimental methodology and apparatus

The inherent optical properties (IOP) generally chosen by the oceanographic community to describe the propagation of light in water are:

- the absorption coefficient $a(\lambda)$ (or the absorption length $L_a = 1/a$);
- the scattering coefficient $b(\lambda)$ (or the scattering length $L_b = 1/b$);
- the attenuation coefficient $c = a + b$ (or the attenuation length $L_c = 1/c = (1/L_a + 1/L_b)^{-1}$);
- the phase scattering function $\chi(\theta,\lambda)$ (also referred to as the volume scattering function).

We note that the IOPs as measured by the oceanographic community do not optimally address the needs of a neutrino telescope. The oceanographers use a well-collimated beam where rays scattered by more than a few mrads are lost, and the attenuation measured is due to the sum of absorption plus scattering. In the case of a large underwater neutrino telescope, such as the KM3NeT, to be deployed in extremely clear and clean sea water, the main light attenuation mechanism is just the absorption since the scattering length is much longer than the absorption length [5]. Underwater neutrino telescopes operate, using uncollimated Cherenkov photons, in an 'open geometry' regime, because their optical modules have a large angle of photon acceptance. In such an open geometry experiment, the optical modules will detect the majority of the Cherenkov photons that are initially generated in the direction toward the module plus some of the scattered photons provided that either of these are not absorbed. Following Bradner et al. [6] we opted to use an open geometry transmissivity meter to measure propagation of light in the sea water. We use the term transmission length L_β ($\beta = 1/L_\beta$ is then the $1/e$ transmission coefficient) in order to avoid confusion with the attenuation length, usually used in experiments with a well-collimated beam. For the series of measurements reported here we have designed and constructed an instrument with 'open geometry', and with an optical path appropriate for transparency measurements in clear waters. We refer to it as the Long Arm Marine Spectrophotometer (the LAMS) and we have used it to make transparency measurements in the deep Ionian Sea.

When the scattering length is much longer than both the absorption length and the measurement distance R, as it is in our case, the transmission coefficient β can be determined experimentally from a combined $1/R^2$ and the Beer–Lambert law [7]:

$$I(\lambda,R) = \frac{I_o(\lambda)}{4\cdot\pi\cdot R^2}\cdot e^{\frac{R}{L_\beta(\lambda)}} \quad (1)$$

Table 1
Dates, locations and depths of measurements.

	Site N4.5D			Site N5.2D	Site CP1	Site CP2
Date (s)	April 19–22, 2008	October 23–24, 25–26, 2008	May 9–10, 2009	October 24–25, 2008	May 6, 2009	May 7, 2009
Coordinates	36°31′N, 21°26′E			36°33′N, 21°08′E	36°11′N, 16°06′E	36°12′N, 15°46′E
Nominal sea depth (m)	4460			5200	3360	3600
Data taking station depth (m)	–	–	–	4900	–	–
	4100	4100	4100	4000	–	–
	3400	3400	3400	–	–	3400
	–	–	3000	3000	3100	3000
	2500	2500	2500	–	2500	2500
	–	2000	2000	2000	2000	2000

where $L_\beta = 1/\beta$ is the transmission length and β the transmission coefficient, $I(\lambda,R)$ is the measured intensity of light of wavelength λ at a distance R from an isotropic light source, and I_0 the intensity of the light source. The relative error in the measurement of β is inversely proportional to the product $\beta \cdot R$:

$$\frac{\Delta\beta}{\beta} = \frac{1}{\beta \cdot R} \cdot \frac{\Delta I}{I} \tag{2}$$

We see that in measurement situations where a small value of $\beta \cdot R$ is used, one may have a large error value even if the light intensity is measured with good accuracy. Therefore, to accurately measure the transmission coefficient β in clear natural waters, where it has small values, we need either an instrument with extreme accuracy in measuring light intensity, or an instrument with a long optical path.

The waters at the sites studied show high transparency [5,7] and the correct measurement of the transmission length is not a simple problem. Commercially available instruments are not well suited for measurements in very clear water; the small length optical base of such instruments (usually no more than 1 m) dictates an increased accuracy of the light intensity measurement.

The LAMS, being an open geometry light measuring system, registers not only direct photons from a light source but also a fraction of the photons scattered in the surrounding water, however note that it does not register those scattered out of the solid angle defined by the point of origin and the detector. The scattering length in clear natural water reaches values of more than 200 m [8]. Since the light path of the LAMS is always much shorter than the scattering length, single scattering of light propagation dominates.

2.1. Long Arm Marine Spectrophotometer (LAMS) – description

We studied the water transparency in an open geometry setup, where an uncollimated light beam was used and where the transmission length was measured. We employed a set of fixed lengths of optical paths and a simple robust method of measuring the light intensity of LED sources, of different wavelengths, at these fixed lengths. The technique employed does not need any external calibration. Moreover, the LAMS design has no movable elements. A rough sketch and a photograph of the LAMS are shown in Fig. 1.

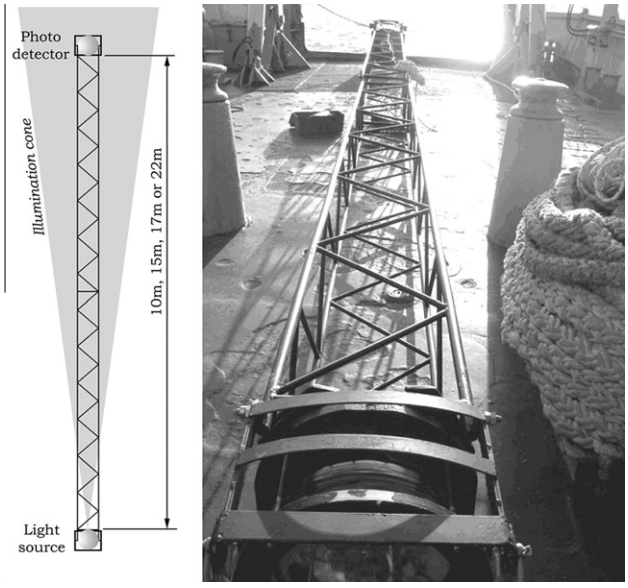

Fig. 1. LAMS – The Long Arm Marine Spectrophotometer. *Left:* Schematic of the apparatus. *Right:* LAMS ready for deployment on the deck of the R/V 'Aegaeo'.

The mechanical frame defining the optical path length consists of five girders attached to each other to form a long linear structure; four girders each being 5 m long and constructed from titanium tubing and one girder 2 m long made from stainless steel tubing. Special attention was paid to alignment issues during construction; the girders were built and welded with the aid of a specially built cradle that allowed for good alignment of the whole structure. The cross-section of the girders is 40 cm × 40 cm. By adding or removing the appropriate girders the overall frame length of the instrument could be varied; during our studies we used the lengths of 10.00, 15.10, 17.17, and 22.27 m for the optical path.

The light source and the light detector are each placed in separate 43.2 cm outer diameter glass spheres [9] (with wall thickness of 1.5 cm) that are fixed on the opposite ends of the frame. In order to minimise unwanted light reflections, the frame, as well as all glass housing parts that are not in the light path, are painted with black matte paint. During deployment the frame was vertical with the light source at the lower end. An additional weight was attached below the frame in order to provide further vertical stability. Alignment stability is assured by the rigid girder structure. Initially, the light source and the light detector were attached at the end of two 5 m long girders and were aligned in the laboratory using a laser beam. The light source and the light detector were mounted on specially constructed frames inside the respective glass spheres and remained fixed throughout the deployments. This was checked by taking calibration measurements before and after deployment for all optical path lengths. The distance between the light source and the detector, as already described, was controlled by adding in-between appropriate girders.

The LAMS is an asynchronous autonomous system. Both source and detector are turned on aboard the ship prior to each deployment and the LAMS is continuously taking data while lowered and recovered. The only parameters controlled from the ship are depth and time. The LAMS is connected with the ship only via the deploying steel wire.

The light source was constructed using eight groups of industrial LEDs. The manufacturer and part number of the various LEDs used are given in Ref. [10]. The LEDs are not monochromatic light sources but emit over a significant spectral region. The spectral distributions of the light sources used are shown in Fig. 2. They were measured in the laboratory using the LED system mounted inside its glass sphere with a commercial diffraction grating spectrophotometer [11], located outside the glass sphere. The wavelengths λ_m for the peak of the light intensity distributions, the Full Width Half Maximum (FWHM) of the spectra and the number of LEDs used for each wavelength group are given in Table 2.

A different number of LEDs was used for each wavelength in order to provide adequate light intensity. The LEDs are mounted on a circuit board arranged inside their glass sphere and are located almost in a circular pattern, within a circle of a radius of 3 cm, as seen in Fig. 3. Over the small angular region subtended by the light detector of the system, a maximum of $\Delta\varphi = \pm 0.15^\circ$ for the shortest optical path used, the intensity is uniform in φ and therefore, in the absence of absorption, it varies as a function of distance, proportionately to $1/R^2$. This absence of angular dependence was determined by measurements in the laboratory, in air [12], where the opening cone of the each LED assembly was found to have a rough bell shape with FWHM greater than 20° in air, or 15° in water, and no significant intensity variation was found over an angular range that matched any possible misalignment, i.e. $\Delta I < 0.5\%$ for $\Delta\theta \approx 2^\circ$ ($\theta = 0^\circ$ defines the direction from the LED source to the centre of light detector).

Each LED group is activated sequentially and is controlled by a microcontroller with a crystal oscillator clock to count time. During a measurement cycle the LEDs of a particular wavelength are

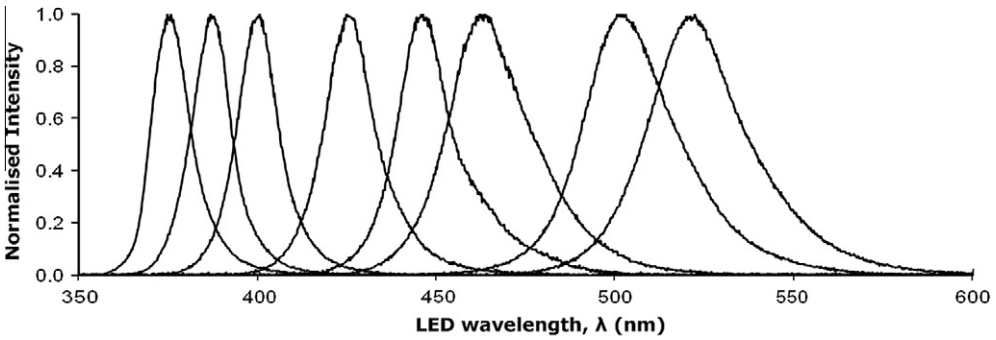

Fig. 2. LED light source spectra (normalised to same max intensity) measured by the spectrophotometer.

Table 2
Light source LED parameters (used in October 2008 and May 2009 deployments). In April 2008 a different LED matrix was used, however the LEDs consisted of the same types, but taken from different manufacturing batches.

Peak intensity wavelength, λ_m (nm)	375.7	385.7	400.3	425.0	445.4	462.6	501.6	519.5
FWHM (nm)	12.9	13.7	13.8	16.6	18.2	26.8	30.7	31.8
Number of LEDs	15	15	7	4	4	7	8	15

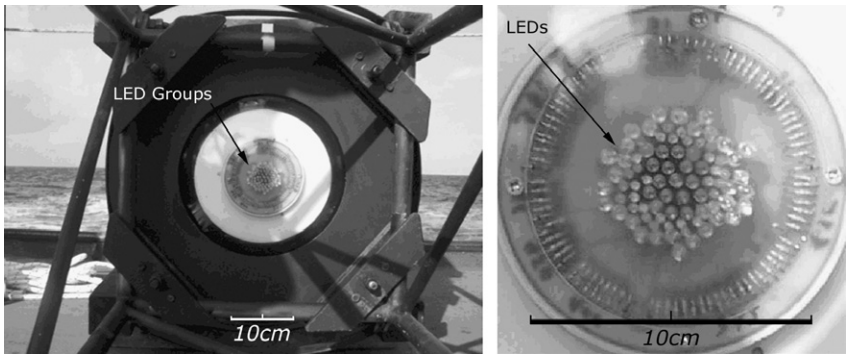

Fig. 3. Light source; cluster of LEDs inside a glass sphere (left), and close-up of the same (right).

turned on for 10 s, then switched off and after 2 s the LEDs of the next wavelength are turned on. Between light cycles a 14 s no-light gap is inserted, and the overall measurement cycle has a period of 110 s. The LEDs are driven from a regulated 5 V source.

The light detector consists of two plane photodiodes [13] with a sensitive area of 18 mm × 18 mm and of very uniform spatial response. The photodiode arrangement in the glass sphere is shown in Fig. 4 together with their spectral response as provided by the manufacturer. They are used to form two independent but identical detectors, running on two different data acquisition channels working with a common clock. In each channel, the current, which is proportional to the light intensity on the detector, is converted to voltage, digitised by a 16 bit ADC. The photodiode current is read 75 times each second. It should be noted that this period, also controlled by a crystal oscillator, is not synchronised with the light source cycling. A 512 MB SD memory card is used for data storage. Data is read-out of this memory and transferred to a laptop PC using a high speed USB port.

Power is supplied by a bank of batteries inside each sphere that houses the source or the detector. The system can operate in a stable autonomous fashion for more than 48 h on a single set of batteries. The glass spheres are equipped with a vacuum port and a 7-pin water-tight electrical receptacle through which the system is controlled (start/stop and on/off for both the source and the detector units, and data read-out for the detector unit).

A typical complete cycle of the system is shown in Fig. 5, where the photodiode response is given in ADC counts. Since all our results are derived from fitting our data to Eq. (1) an absolute normalization of the light intensity is not required.

To reduce the noise the response is heavily damped in the electronics. This explains the long RC time constant in the rising and falling edges. In each light-on measuring period of 10 s there are some 750 measurements of the intensity; to avoid complications due to the RC time constant of the detector electronic circuit, we only utilize the data of the last 2/3 of each measuring period, i.e. we use the last 495 samples. Some light sources display a time dependence of their intensity which decreases as a function of time; such variations were taken into account by fitting a straight line to the data of each measuring period. The value of the fit at the latest time of each measuring period gave the corresponding light intensity. We note that this time dependence of the intensity is characteristic for each LED assembly at a given wavelength and does not depend on the length of the optical light path. Therefore it does not affect the intensity fit to the different optical paths, provided the same data analysis procedure is followed. The intensity thus derived was averaged over many cycles (10–20 complete 110 s cycles were taken at each depth and wavelength) and as a result the statistical error on the light intensity is very small. A small zero offset, determined by the residual dark current measurements during the no-light gap was subtracted.

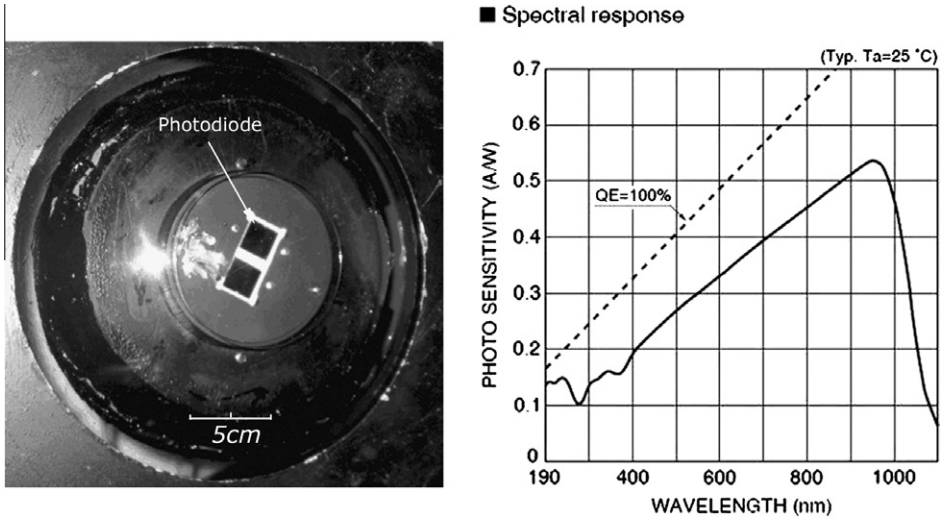

Fig. 4. Light detector system; the two Si large area Hamamatsu S6337-01 Si photodiodes (left) and their spectral response [13] (right).

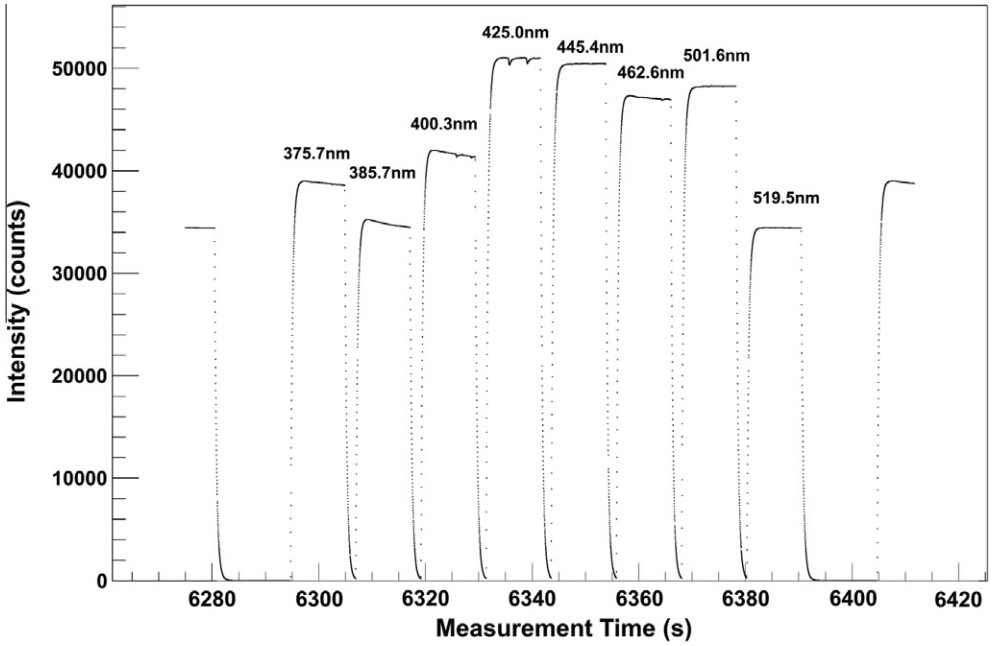

Fig. 5. Typical cycle of raw data obtained by the LAMS, at the N45 site at 4100 m deep in October 2008. This data is from a configuration with optical path of 10 m and shows that even in this case, where the light intensities are highest, the ADC is not saturated.

Another feature of the intensity graphs, Fig. 5, is the presence of occasional small downwards transients. The time structure of these transients indicates that they are due to small decreases of the light intensity reaching the detector. We attribute these to small flakes of particulate matter floating in the field of view of our light sensor. We found that removing those transients does not alter the value of the reported light intensity of each measuring period. Such transients were seen in all of the deployments and are consistent with the frequency and size of observed larger particulate matter seen in video surveys of the deep sea [14].

3. Measurement details and data analysis

In a neutrino underwater telescope, such as the proposed KM3NeT, the light detecting optical modules are sparsely deployed in the deep sea and thus, as already mentioned, we are in the situation of an open geometry where there is no collimation of the detected light. Therefore the use of an uncollimated beam, such as the one of the LAMS, is appropriate for a measurement of the transmission of light over different lengths of water paths. The light intensities of the LED sources as detected by the photodiode, $I(\lambda,R)$, at various but fixed distances (light paths) R between the source and the detector are recorded and compared to each other. As a result we do not need any external or absolute calibration.

Laboratory tests of the LAMS in air show that the attenuation of light intensity is almost totally due to a geometrical spreading of the beam and follows with high accuracy the $1/R^2$ law. The LAMS was tested in air before and after each deployment and its characteristics remained the same. Given the fact that the attenuation length in air for a clear standard atmosphere is 4–7 km for the visible light range [15], our instrument is not of sufficient length to reliably measure it.

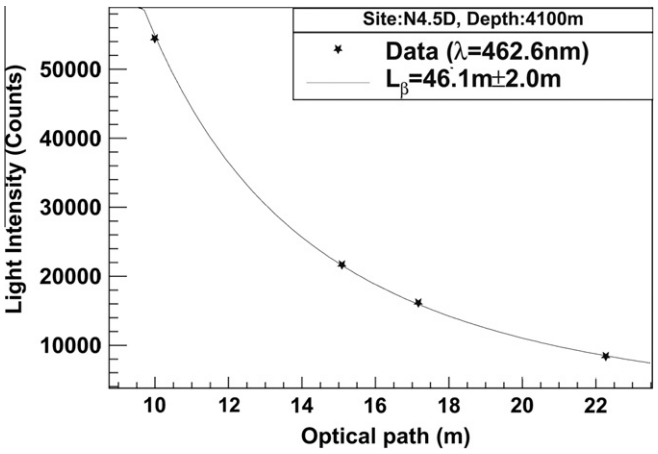

Fig. 6. Typical result of the fit. The data are points with error bars (not visible because they are too small), and the line is the fit to Eq. (1).

The intensity data are divided in data sets. Each set combines all the data for a particular depth for each stationary deployment, for each specific LAMS length, and for each LED source (i.e. wavelength range). The light intensity measurements were combined and averaged and as a result instrumental noise is highly suppressed. We use this mean intensity $I(\lambda, R)$ and its statistical error for further analysis. We have added in quadrature an additional 0.5% error in the intensity as an estimate of systematic uncertainties of the angular dependence as described in Section 2.1. Then, for each set, the intensity data for each wavelength range are fit to Eq. (1). We have allowed for a ΔR variation in the arm lengths of $\Delta R = \pm 2$ cm for 10.00 m arm length, $\Delta R = \pm 3$ cm for 15.10 m, $\Delta R = \pm 3$ cm for 17.17 m, and $\Delta R = \pm 4$ cm for 22.27 m, in the fit to account for any uncertainty in the light path and for the thickness of the curved envelopes of the glass spheres. From the fit we determine I_0 (which we use as a check of the stability of the source) and the transmission length L_β and its error for each wavelength. The data follow the combined $1/R^2$ and the Beer–Lambert law very well; a typical example of a fit is shown in Fig. 6.

The system was suspended from a 12 mm diameter steel wire cable and was lowered into the sea, at a speed of less than 1 m/s, from the deployment vessel. The depth where the LAMS was located was calculated from the length of the deployed steel wire using the ship's wire length measuring device.[1] The measured length using this device was compared with the depth determined from a pressure sensor attached on the LAMS and the difference was less than 10 m. The duration of the measurement at each station was about 20 min, while at the deepest stations the measurement duration was about 40 min. After each recovery, the length of the LAMS light path was changed on deck by adding girder sections, as described above, while the data were recovered from the LAMS memory.

4. Results

Tables 3–6 show the transmission length measurements for all deployments where the LAMS was stationary. Since the LAMS keeps taking data throughout its descent and ascent we have collected data at all depths while the instrument was moving. We are not presenting at this time results from the descending and ascending periods; the analysis of these data is ongoing and will provide a more detailed profile of the light transmission as a function of sea depth. Tables 7 and 8 show the ratios of the transmission lengths at the sites measured in May 2009 for the depths around 3000 m and also at the deepest depths, where the neutrino telescope elements will be located. Fig. 7 shows the transmission length measurements from the Pylos sites.

The data are presented as being taken at the peak of the spectral distribution of each light source. We have not taken into account the spectral shape of the various LED sources, nor have we integrated over the spectral response of the photodiode.

5. Discussion

We will focus on three aspects of the variation seen in our measurements of the transmission length:

- depth dependence, where the transparency changes with depth,
- temporal effects, i.e. the transparency depends on the season, and
- site dependence, i.e. the variation in the transmission length for different sites but at similar depths but only for measurements taken within a few days of each other.

5.1. Depth dependence of the transmission

The variation of the transmission length for various depths is about 2–5 m with shorter transmission lengths for shallower waters and is about the same at all sites. The transmission length always reaches a maximum at depths 3000–3400 m. These data are consistent with the results of previous measurements at three different nearby sites [16], performed with an early version of a similar system, albeit our measurements always lie at the lower limit of the uncertainty of the earlier data, as shown in Fig. 8.

The measurements reported here correlate well with the data of Ref. [2], where the depth dependence of hydrological and optical parameters are explained by the presence of waters of different origin at different depths: at ~3300 m there is water that originates in the Cretan Sea and thus is characterised by higher salinity, temperature and optical transparency; at depths below ~3600 m, there is water of Adriatic origin as is indicated by the decreasing salinity and water transparency. This Adriatic water is newly formed, i.e. it was recently at the surface and has been sub-ducted at those depths due to dense water formation during some recent winter season. At depths greater than ~5000 m the oxygen values are decreasing and this is indicative of some isolated old Adriatic water mass that is found in the bottom layers of the N5.2D site.

5.2. Temporal effects

In Fig. 9 we show the temporal variability of the water transparency at the Pylos site. The data of April 2008 and October 2008 are consistent with each other, however both of these spectra differ from the one of May 2009, mainly for the wavelengths 425.0 and 462.9 nm (see Fig. 7). We cannot show any temporal variability at Capo Passero site since data were taken with the LAMS only in May 2009; however in [18] it is reported that at the of Capo Dassero there are considerable time variations in absorption spectra of deep water for the wavelengths 412 and 440 nm.

It is well known from oceanographic studies that variations of the optical parameters of sea water depend on the wavelength and are caused by changes in the water's composition. As noted in [7], in the wavelength range of 390–470 nm the contribution to scattering from submersed particles dominates, while dissolved organic materials (the so-called 'yellow substance') account for 83–95% of the light attenuation in sea water. Thus, the variability of the transmission length of deep water is almost completely caused by changes in concentration of submersed particles and

[1] A pulley with a turn-counting unit.

Table 3
Transmission length, L_β, in metres at site **N4.5D, April 2008** deployments. The reader should note that different light sources with slightly different wavelength are used in April 2008 compared to those used in the subsequent deployments.

Depth (m)	Date	λ (nm)							
		374.8	379.8	402.2	424.2	445.6	461.2	504.0	519.1
2500	April 08	20.8 ± 0.2	25.6 ± 0.3	31.3 ± 0.8	42.2 ± 0.8	41.7 ± 0.8	42.9 ± 1.5	27.9 ± 0.4	22.5 ± 0.3
3400	April 08	20.8 ± 0.2	24.9 ± 0.3	31.1 ± 0.8	42.8 ± 0.9	42.6 ± 0.9	45.7 ± 1.7	28.1 ± 0.4	22.3 ± 0.3
4100	April 08	20.6 ± 0.2	22.5 ± 0.3	28.0 ± 0.7	41.4 ± 0.8	41.5 ± 0.8	40.1 ± 1.3	27.7 ± 0.4	21.1 ± 0.2

Table 4
Transmission length, L_β, in metres at site N5.2D, October 2008 deployments.

Depth (m)	λ (nm)							
	375.7	385.7	400.3	425.0	445.4	462.6	501.6	519.5
2000	21.5 ± 0.3	25.4 ± 0.3	29.8 ± 0.4	40.3 ± 0.8	42.3 ± 0.8	42.8 ± 0.9	30.2 ± 0.5	21.3 ± 0.2
3000	21.6 ± 0.3	26.0 ± 0.3	30.7 ± 0.5	41.8 ± 0.8	44.7 ± 0.9	45.1 ± 0.9	30.8 ± 0.5	21.6 ± 0.3
4000	20.6 ± 0.2	24.3 ± 0.3	28.5 ± 0.4	38.6 ± 0.7	40.9 ± 0.8	41.7 ± 0.8	29.4 ± 0.4	20.9 ± 0.2
4900	20.3 ± 0.2	24.1 ± 0.3	28.3 ± 0.4	38.0 ± 0.7	40.4 ± 0.8	40.6 ± 0.8	29.3 ± 0.4	20.6 ± 0.2

Table 5
Transmission length, L_β, in metres at site N4.5D, October 2008 and May 2009 deployments.

Depth (m)	Date	λ (nm)							
		375.7	385.7	400.3	425.0	445.4	462.6	501.6	519.5
2000	October 08	21.2 ± 0.2	25.4 ± 0.3	29.3 ± 0.4	40.4 ± 0.8	40.5 ± 0.8	42.2 ± 0.8	29.8 ± 0.4	21.0 ± 0.2
	May 09	20.8 ± 0.5	24.0 ± 0.7	28.4 ± 0.8	34.7 ± 1.2	39.4 ± 1.6	42.0 ± 1.7	27.8 ± 0.8	20.9 ± 0.5
2500	October 08	21.6 ± 0.3	26.1 ± 0.4	30.5 ± 0.5	42.7 ± 0.9	42.5 ± 0.9	44.6 ± 0.9	30.6 ± 0.5	21.4 ± 0.2
	May 09	21.7 ± 0.5	25.4 ± 0.6	30.0 ± 0.9	36.3 ± 1.3	41.9 ± 1.7	45.5 ± 2.0	28.6 ± 0.8	21.4 ± 0.5
3000	May 09	21.9 ± 0.5	25.7 ± 0.7	30.5 ± 1.0	37.8 ± 1.5	43.8 ± 1.9	47.2 ± 2.2	29.3 ± 0.9	21.5 ± 0.6
3400	October 08	21.4 ± 0.2	25.9 ± 0.3	30.1 ± 0.5	43.0 ± 0.9	42.2 ± 0.8	43.8 ± 0.9	30.4 ± 0.5	21.5 ± 0.2
	May 09	21.9 ± 0.5	25.7 ± 0.7	30.4 ± 1.0	38.2 ± 1.4	44.3 ± 1.9	47.8 ± 2.2	29.8 ± 0.9	21.9 ± 0.6
4100	October 08	20.5 ± 0.2	24.7 ± 0.3	28.4 ± 0.4	39.7 ± 0.8	39.8 ± 0.8	41.5 ± 0.8	28.0 ± 0.4	20.9 ± 0.2
	May 09	21.0 ± 0.5	24.8 ± 0.7	29.2 ± 0.9	36.0 ± 1.3	42.3 ± 1.8	46.1 ± 2.0	28.7 ± 0.8	21.3 ± 0.5

Table 6
Transmission length, L_β, in metres at sites CP1 and CP2, May 2009 deployments.

Depth (m)	Site	λ (nm)							
		375.7	385.7	400.3	425.0	445.4	462.6	501.6	519.5
2000	CP1	19.6 ± 0.4	22.9 ± 0.6	27.1 ± 0.7	32.6 ± 1.1	37.8 ± 1.4	39.4 ± 1.6	26.7 ± 0.8	20.8 ± 0.5
	CP2	17.6 ± 0.4	20.4 ± 0.5	23.8 ± 0.6	28.6 ± 0.8	33.1 ± 1.2	35.8 ± 1.3	24.9 ± 0.7	19.4 ± 0.4
2500	CP1	20.1 ± 0.5	23.6 ± 0.6	28.1 ± 0.8	34.5 ± 1.2	40.2 ± 1.6	42.4 ± 1.8	27.9 ± 0.8	21.4 ± 0.5
	CP2	18.2 ± 0.4	21.2 ± 0.5	24.8 ± 0.7	30.4 ± 0.9	34.9 ± 1.3	38.0 ± 1.4	25.8 ± 0.7	19.9 ± 0.4
3100	CP1	19.9 ± 0.4	23.2 ± 0.6	27.8 ± 0.8	34.6 ± 1.2	41.5 ± 1.7	44.1 ± 1.9	28.5 ± 0.8	21.8 ± 0.5
3000	CP2	19.5 ± 0.4	23.0 ± 0.5	27.3 ± 0.8	34.1 ± 1.2	39.6 ± 1.6	43.7 ± 1.8	27.6 ± 0.8	21.1 ± 0.5
3400	CP2	18.6 ± 0.4	21.8 ± 0.5	25.6 ± 0.7	32.4 ± 1.1	38.5 ± 1.5	42.0 ± 1.7	27.1 ± 0.8	20.9 ± 0.5

Table 7
Comparison (ratios of transmission lengths) at the three sites measured in May 2009, for similar depths (i.e. 3000–3100 m).

Ratio	λ (nm)							
	375.7	385.7	400.3	425.0	445.4	462.6	501.6	519.5
N4.5D (3000 m)–CP1 (3100 m)	1.10 ± 0.03	1.11 ± 0.04	1.10 ± 0.05	1.09 ± 0.06	1.06 ± 0.06	1.07 ± 0.07	1.03 ± 0.04	0.99 ± 0.04
N4.5D (3000 m)–CP2 (3000 m)	1.12 ± 0.03	1.12 ± 0.04	1.12 ± 0.05	1.11 ± 0.06	1.11 ± 0.07	1.08 ± 0.07	1.06 ± 0.04	1.02 ± 0.04

of the 'yellow substance'. Temporal variations of the water optical parameters at the Pylos and the Capo Passero areas can be explained as being the result of underwater processes when water masses stratify due to density differences but also undergo some vertical migration through dynamic circulation structures (cyclones or anticyclones) present in the Eastern Mediterranean [17].

5.3. Site dependence

Even though the transmission length differences between the N4.5D and the N5.2D sites are small (about 1 m as seen in Fig. 7b and c), the transmission length at Capo Passero is about 10% shorter than the transmission length at the Pylos site. However, the

Table 8
Comparison (ratios of transmission lengths) at the three sites measured in May 2009, for the maximum deployment depths at each site.

Ratio	λ (nm)							
	375.7	385.7	400.3	425.0	445.4	462.6	501.6	519.5
N4.5D (4100 m)–CP1 (3100 m)	1.06 ± 0.03	1.07 ± 0.04	1.05 ± 0.04	1.04 ± 0.05	1.02 ± 0.06	1.05 ± 0.06	1.01 ± 0.04	0.98 ± 0.03
N4.5D (4100 m)–CP2 (3400 m)	1.13 ± 0.04	1.14 ± 0.04	1.14 ± 0.05	1.11 ± 0.06	1.10 ± 0.06	1.10 ± 0.07	1.06 ± 0.04	1.02 ± 0.03

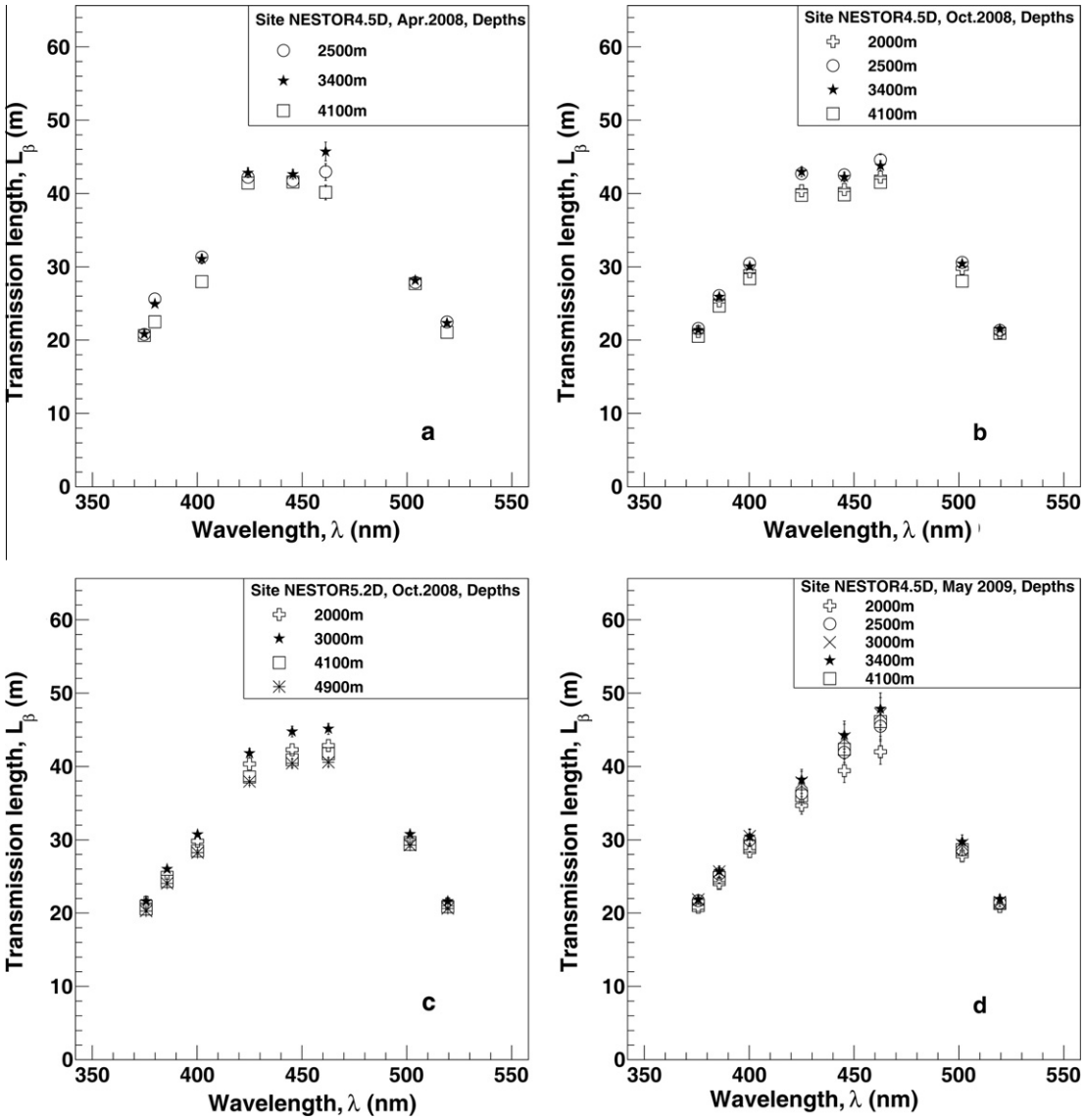

Fig. 7. Data obtained in the Pylos N4.5D and N5.2D sites (if an error bar is not shown, then it is smaller than the symbol size). (a) April 2008, N4.5D site; (b) October 2008. N4.5D site; (c) October 2008, N5.2D site; (d) May 2009. N4.5D site.

spectral shapes of the transmission length at all sites are very similar, as shown in Fig. 10.

5.4. Comparison of transmission and attenuation spectra

A comparison of the transmission length spectrum with the spectrum of the attenuation length measured with a transmissometer configuration using a highly collimated beam [19] (see Fig. 11a) shows that the transmission length exceeds the attenuation length at wavelength $\lambda < 490$ nm, but at $\lambda > 490$ nm transition length coincides with attenuation length of pure sea water. This feature can be explained by the characteristics of light scattering and absorption by sea water. It is known that for long-wavelengths, scattering is very weak and in that region of the spectrum the attenuation is mainly due to the absorption of photons by water molecules [7]. The presence of dissolved impurities and suspended particles does not have any effect. However, with decreasing wavelength the scattering increases, and in the violet region close to the UV the absorption of photons by molecules of dissolved organic material ('yellow substance') begins to dominate while absorption by water molecules has become negligible.

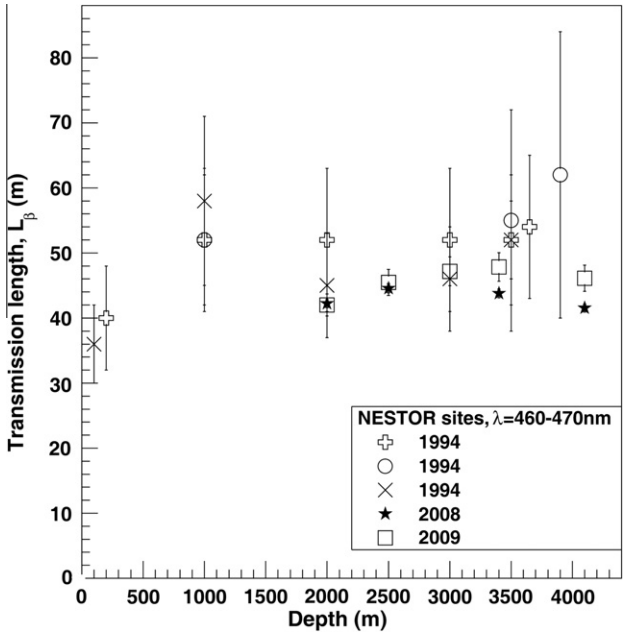

Fig. 8. Data obtained at the Pylos N4.5D site. Comparison of the LAMS data at 460–470 nm wavelength (October 2008, with results from 1994 for three different nearby sites [16]) (if an error bar is not shown, then it is smaller than the symbol size).

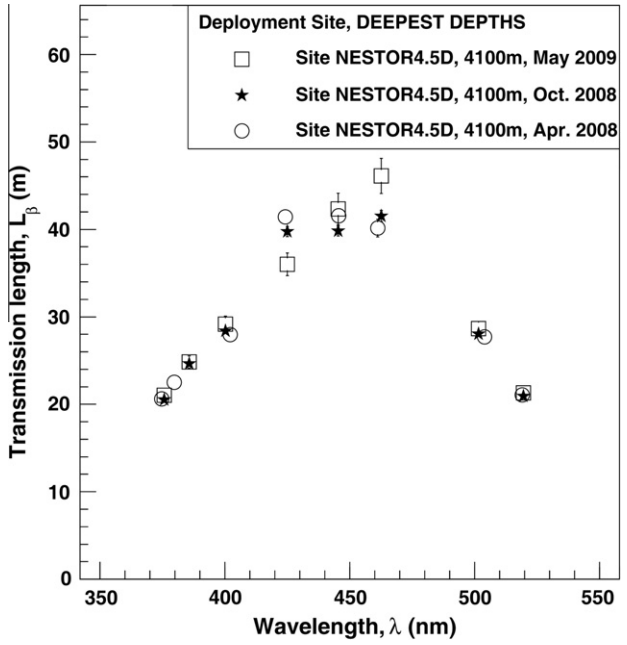

Fig. 9. Transmission length measured in April 2008, October 2008, and May2009 at the Pylos N4.5D site; depth 4100 m (if an error bar is not shown, then it is smaller than the symbol size).

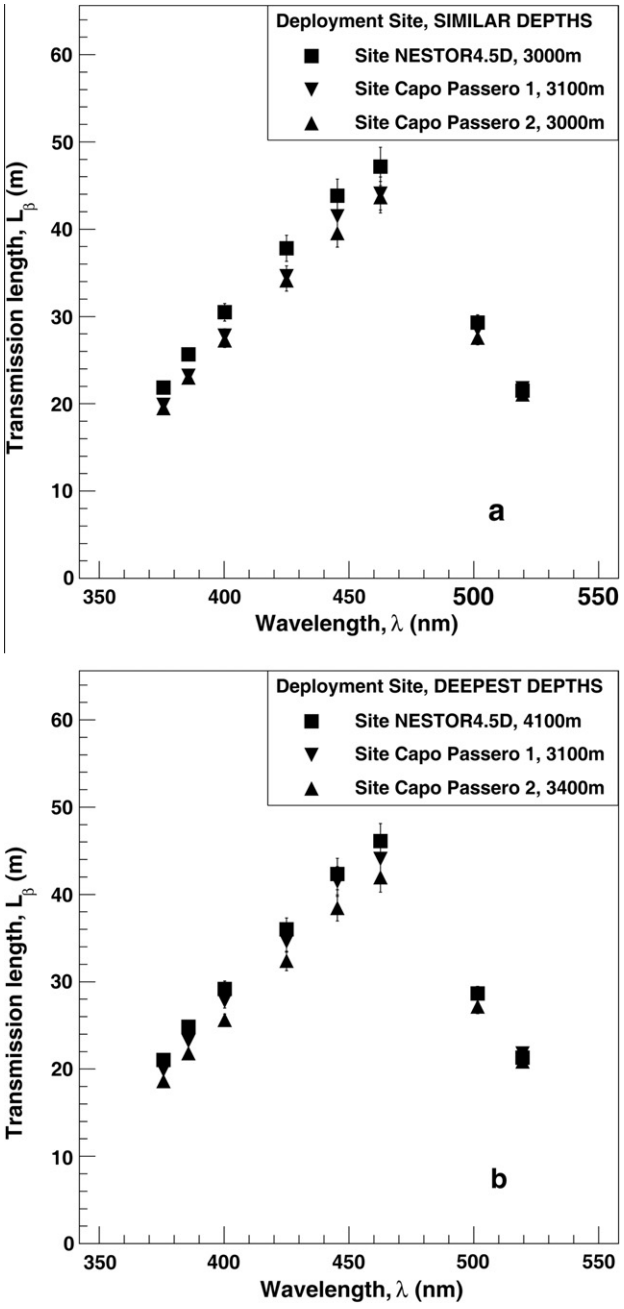

Fig. 10. Transmission length versus wavelength at the Capo Passero and Pylos sites (if an error bar is not shown, then it is smaller than the symbol size). *a*: for similar depths; *b:* for the maximum deployment depths (at about 300 m above seabed).

6. Conclusions

The transparency of deep sea water has been measured with the LAMS (Long Arm Marine Spectrophotometer) in two well separated sites in the Western and Eastern Ionian Sea in order to study optical parameters at locations where the KM3NeT large underwater neutrino telescope may be deployed. An uncollimated light source of eight different wavelength ranges was used to measure the optical parameters in the spectral region where the optical detection units of the neutrino telescope (bi-alkali photocathode photomultipliers) have quantum efficiency larger than a few percent.

The values of the transmission length measured in the Eastern Ionian Sea (Pylos N4.5D and N5.2D sites) are in good agreement with each other and with earlier measurements. Light transmission lengths in the Eastern Ionian are 10% longer than the ones measured in the Western Ionian. The optical properties at the Pylos site have a weak depth dependence but are laterally homogeneous over a large geographic region ($\sim$1000 km^2), and although there are $\sim$15% seasonal variations for violet-blue wavelengths the transmission lengths are compatible with being constant over the investigated multiyear timescale, 1994–2009.

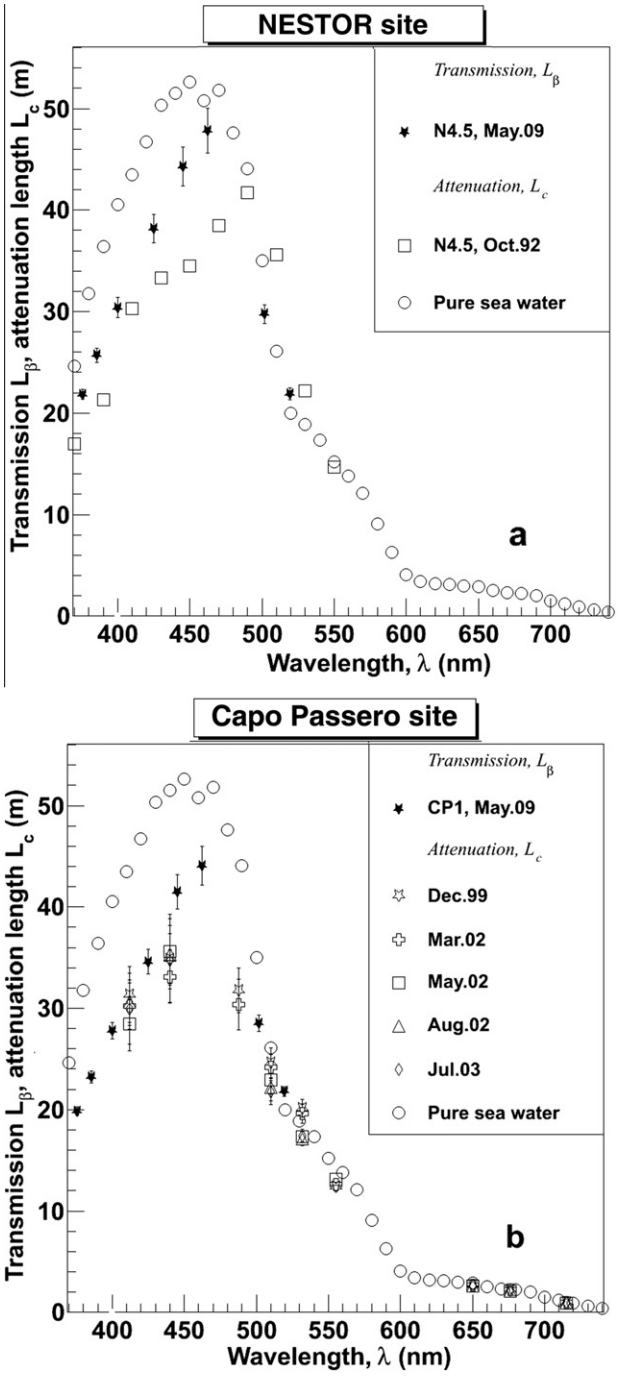

Fig. 11. Transmission or attenuation lengths at the Pylos and Capo Passero sites. (a) Transmission lengths: at N4.5D site at 3400 m, May 2009 (triangles); Attenuation lengths at depth 3800 m, October 1992 (squares [19]). (b) CP1 site, Transmission lengths at 3100 m, May 2009 (triangles); attenuation lengths at 2850–3250 m from [18], December 1999 (open circles), March 2002 (open crosses), May 2002 (open squares), August 2002 (open triangles) and July 2003 (open diamonds). The attenuation lengths for pure sea water are from [8].

In a broad wavelength range the transmission length coincides systematically with the attenuation length, while in the region between, roughly, 420–480 nm it exceeds it. The large difference between the two, at around 510 nm, is probably due to the very steep slope of both attenuation and transmission length, combined with small uncertainty in the wavelengths of the different light sources used in 1992 and 2009.

Acknowledgements and dedication

We thank our colleagues from the Hellenic Centre for Marine Research for their help, especially the former Director George Chronis as well as the Captain, the Officers and the Crew of the R/V "Aegaeo". We also thank our colleagues John Learned of the University of Hawaii and Hank Crawford of the University of California, Berkeley, for their overall help and for many helpful discussions throughout many years. Further thanks go to H. Crawford and his undergraduate advisee M. Ng for providing us with the prototype electronics circuit and Mssrs T. Athanasopoulos, J. Kiskiras and E. Maniatis for implementing the necessary modifications. We also thank our mechanical engineering team for their contributions to designing and constructing a robust reliable spectrometer that performed well despite the punishment of the deep sea, special thanks go to N. Arvanitis, A. Darsaklis, T. Michos, J. Roussos, A. Vougioukas and D. Vakontios.

Parts of this Research have been funded by a Centre of Excellence award of the General Secretariat for Research and Technology of the Ministry of Development of Greece, and by the EU in the 6th 10 Framework Program under Contract Number 011937. We also thank the Hamamatsu Photonics Co for providing the photodiodes gratis.

We dedicate this paper to the memory of our good friend, mentor, and collaborator, Hugh Bradner, Professor of Engineering Physics and Geophysics, Institute of Geophysics and Planetary Physics, Scripps Institution of Oceanography, University of California, San Diego and former Associate Director for Particle Physics, Lawrence Radiation Laboratory.

References

[1] A. Achterberg et al., First year performance of the IceCube neutrino telescope, Astropart. Phys. 26 (2006) 155–173. Website <http://icecube.wisc.edu>.
[2] KM3NeT Conceptual Design Report, April 2008, 118 p., ISBN 978-90-6488-031-5. Website: <http://www.km3net.org/>.
[3] L.K. Resvanis for the NESTOR collaboration, NESTOR: a neutrino particle astrophysics underwater laboratory for the Mediterranean, in: V.J. Stenger, J.G. Learned, S. Paksava, X. Tata, (Eds.), Proceedings of the High Energy Neutrino Astrophysics Workshop, Hawaii, vol. 325, World Scientific, Singapore, 1992. Website: <http://www.nestor.noa.gr>.;
G. Aggouras et al., A measurement of the cosmic-ray muon flux with a module of the NESTOR neutrino telescope, Astropart. Phys. 23 (2005) 377–392;
G. Aggouras et al., Operation and performance of the NESTOR test detector, Nucl. Instrum. Methods Phys. Res. Sect. A 552 (3) (2005) 420–439.
[4] E. Migneco et al., The NEMO project, in: Proceedings of the VLVnT Workshop, NIKHEF, Amsterdam, 5–8 October 2003, pp. 5–10. Website: <http://nemoweb.lns.infn.it>.
[5] N.G. Jerlov, Optical Oceanography, American Elsevier, New York, 1968;
A.S. Monin, Ocean Optics; Physical Optics of the Ocean. Chapter 7, Paragraph 7.1 (Scattering properties of sea water), pp. 167–179 (in Russian).;
M. Jonasz, G.R. Fournie, Light Scattering by Particles in Water, Theoretical and Experimental Foundations, 2007 Elsevier Inc., Chapter 4, Paragraph 4.4.2.1 (Scattering coefficients), pp. 210–216.
[6] H. Bradner, G. Blackinton, Appl. Opt. 23 (1984) 1009;
H. Bradner et al., Attenuation of light in clear deep ocean water, in: L.K. Resvanis (Ed.), Proceedings of the 2nd NESTOR International Workshop, Pylos, Greece, October 19–21, 1992, p. 247.
[7] A.S. Monin (Ed.), Ocean Optics; Physical Optics of the Ocean, Nauka, Moscow, 1983. pp. 225, 226, and 234 (in Russian).
[8] R. Smith, K. Baker, Optical properties of the clearest natural waters (200–800 nm), Appl. Opt. 20 (1981) 177 (Derived from Table I).
[9] Made of a borosilicate glass (Pyrex), by Teledyne Benthos Inc., North Falmouth, MA, USA.
[10] "375 nm" NSHU590A, Nichia Corp., Tokushima, Japan; "385 nm" LED385, Roithner Lasertechik GmbH, Vienna, Austria; "400 nm" LED3-UV-400-30, Bivar Inc., Irvine, California, USA; "425 nm" LED425-6-3U, Roithner Lasertechik GmbH; "450 nm" LED450-01U, Roithner Lasertechik GmbH; "470 nm" L-7104QBC-D Kingbright Elec. Co., Taipei, Taiwan; "495 nm" NSPE510S Nichia Corp.; "525 nm" NSPG510S Nichia Corp.
[11] Model USB4000 Spectrophotometer, manufactured by Ocean Optics Inc., Dunedin, Florida, USA. As used the USB4000 was equiped with a 25 μm slit and a UV grating (Grating type H1, 1600 grooves/mm, useful range 200–575 nm, peak sensitivity 300 nm) and had an intrinsic FWHM resolution of 1.3 nm. The data of Fig. 2 have not been corrected for the spectral dependence of the response of the USB4000.

[12] S. Koutsoukos et al., NESTOR-Note-010.2009, unpublished.;
E. Chaniotakis, A. Hadjitheodorou, G. Karathanasis, NESTOR-Note-075.2009, unpublished.
[13] Large Area Si Photodiode Part No. S6337-01, Hamamatsu Photonics K.K., Hamamatsu, Japan.
[14] I.G. Priede, private communication, based on the deployment of an ISIT camera in the Ionian Sea. The technique is described in A.J. Jamieson et al., Illumination of trawl gear by mechanically stimulated bioluminescence, Fish. Res. 81 (2006) 276.
[15] See Table 7.4 in S.L. Valley (Ed.), Handbook of geophysics and space environments, Air Force Cambridge Research Center, Bedford, Mass., USA, and also McGraw-Hill, New York, 1965, also presented in Fig. 7-3 of R.W. Engstrom (Ed.), Electro-Optics Handbook, RCA Corp., Technical Series EOH-11, Lancaster, Penn., 1974.
[16] E.G. Anassontzis et al., Light transmissivity in the NESTOR site, Nucl. Instrum. Methods A349 (1994) 242–246.
[17] H. Kontoyiannis et al., Water-mass structure and deep currents in the NESTOR area, 2009, 7p., Contribution to the KM3NeT Design Study, Work Package 5, unpublished.
[18] G. Riccobene et al., Deep sea water inherent optical properties in the Southern Ionian Sea, Astropart. Phys. 27 (2007) 1–9.
[19] S.A. Khanaev et al., Measurements of water transparency South-West of Greece, in: L.K. Resvanis (Ed.), Proceedings of the 2nd NESTOR International Workshop, Pylos, Greece, October 19–21, 1992, p. 253.